ATMOSPHERIC DISPERSION IN THE ARCTIC: WINTER-TIME BOUNDARY-LAYER MEASUREMENTS

ALEX GUENTHER and BRIAN LAMB

Laboratory for Atmospheric Research, Washington State University, Pullman, WA 99164-2910 U.S.A.

(Received in final form 14 June, 1989)

Abstract. The winter-time arctic atmospheric boundary layer was investigated with micrometeorological and SF_6 tracer measurements collected in Prudhoe Bay, Alaska. The flat, snow-covered tundra surface at this site generates a very small (0.03 cm) surface roughness. The relatively warm maritime air mass originating over the nearby, partially frozen Beaufort Sea is cooled at the tundra surface resulting in strong (4 to 30 °C · (100 m)$^{-1}$) temperature inversions with light winds and a persistent weak (1 to 2° C · (100 m)$^{-1}$) surface inversion with wind speeds up to 17 m s^{-1}. The absence of any diurnal atmospheric stability pattern during the study was due to the very limited solar insolation. Vertical profiles were measured with a multi-level mast from 1 to 17 m and with a Doppler acoustic sounder from 60 to 450 m. With high wind speeds, stable layers below 17 m and above 300 m were typically separated by a layer of neutral stability. Turbulence statistics and spectra calculated at a height of 33 m are similar to measurements reported for non-arctic, open terrain sites and indicate that the production of turbulence is primarily due to wind shear. The distribution of wind direction recorded at 1 Hz was frequently non-Gaussian for 1-hr periods but was always Gaussian for 5-min periods. We also observed non-Gaussian hourly averaged crosswind concentration profiles and assume that they can be modeled by calculating sequential short-term concentrations, using the 5-min standard deviation of horizontal wind direction fluctuations (σ_θ) to estimate a horizontal dispersion coefficient (σ_y), and constructing hourly concentrations by averaging the short-term results. Non-Gaussian hourly crosswind distributions are not unique to the arctic and can be observed at most field sites. A weak correlation between horizontal (σ_v) and vertical (σ_w) turbulence observed for both 1-hr and 5-min periods indicates that a single stability classification method is not sufficient to determine both vertical and horizontal dispersion at this site. An estimate of the vertical dispersion coefficient, σ_z, could be based on σ_ϕ or a stability classification parameter which includes vertical thermal and wind shear effects (e.g., Monin–Obukhov length, L).

1. Introduction

A smooth, snow-covered surface, extremely cold temperatures, and a lack of solar insolation are typical of winter in polar regions. These conditions differ from what is typically observed in the lower latitudes and can have a significant impact on the structure of the atmospheric boundary layer (ABL), which is influenced by factors such as surface roughness and thermal stability. Extremely low surface roughness and persistent thermal stability have been observed in both arctic (Weller and Holmgren, 1974) and antarctic (Dalrymple *et al.*, 1966) regions. Although the characterization of the ABL in polar regions is of interest from a fundamental basis, industrial development in the Arctic has created an important applied aspect. In order to develop appropriate air quality control strategies, we must have a clear understanding of how the arctic boundary layer affects pollutant dispersion.

In this paper, we present measurements of turbulence and boundary-layer structure over open winter-time tundra with an emphasis upon the implications of

Boundary-Layer Meteorology **49**: 339–366, 1989.

these observations for pollutant dispersion modeling. Vertical profiles of mean wind speed, wind direction and temperature are described, in addition to fluctuations in these quantities. Dispersion coefficients are estimated and compared with our open terrain tracer plume measurements. This work is part of an arctic dispersion modeling program supported by the EPA Cold Climate Research Program. In other aspects of the program, we have investigated plume downwash and dispersion at an arctic industrial site using wind-tunnel model studies (Guenther *et al.*, 1989a) and atmospheric tracer field studies (Guenther *et al.*, 1989b; Rickel *et al.*, 1989).

2. Description of the Field Study

The field site was located within the Prudhoe Bay oilfield (70° 15′ N, 148° 30′ W) about 10 km inland from the Beaufort Sea. The area is part of the Arctic Coastal Plain in Alaska which contains several producing and potential oilfields within an ecologically sensitive tundra biome. The Coastal Plain has a uniformly flat terrain with a very gradual slope ($\approx$0.1%) from the Brooks mountain range to the Beaufort Sea in the north. There are numerous small, shallow lakes which are a result of the poorly defined drainage systems in the region. Typical relief in the undisturbed areas is several meters although widely scattered pingos (small isolated hills produced by frost heaves) may reach heights of 15 m. Roads, pipelines, well pads, and oil gathering facilities dominate the relief within the Prudhoe Bay oilfield. This site is representative of Northern Alaska and other arctic regions with proposed or existing resource development activity.

Mosses, sedges and lichens are the dominant plant species at the field site. The tallest plants are willows which occasionally reach heights of 25 cm but are usually prostrate (Walker and Webber, 1979). The continual presence of a snow covering between September and May provides a smooth surface over the tundra vegetation. Winds are predominantly from the east or west throughout the year and are usually between 5 and 7 m s^{-1} with very low winds (1.5 m s^{-1}) occurring 10% of the time and very high winds (>12.5 m s^{-1}) occurring 10% of the time (Lamb and Allwine, 1986). High winds are associated with winter storms and blowing, drifting snow. From the perspective of pollutant dispersion, the predominance of moderate to high winds in the arctic implies the likelihood of significant plume downwash and a corresponding increase in surface pollutant concentrations due to the low turbine stacks associated with the arctic oil production facilities.

Field measurements were conducted from October 23 to November 9, 1987 at the Prudhoe Bay oilfield sites shown in Figure 1. The field sites were covered with snow and the Beaufort Sea was frozen out to 10 to 20 km from the coast (Hanzlick *et al.*, 1988). During the field study, 15-min averaged vertical profiles of wind and temperature in the surface layer were measured continuously with an instrumented mast located in open tundra at well pad G (see Figure 1). At the same time, upper-level winds, averaged over 15 minutes, were measured on a

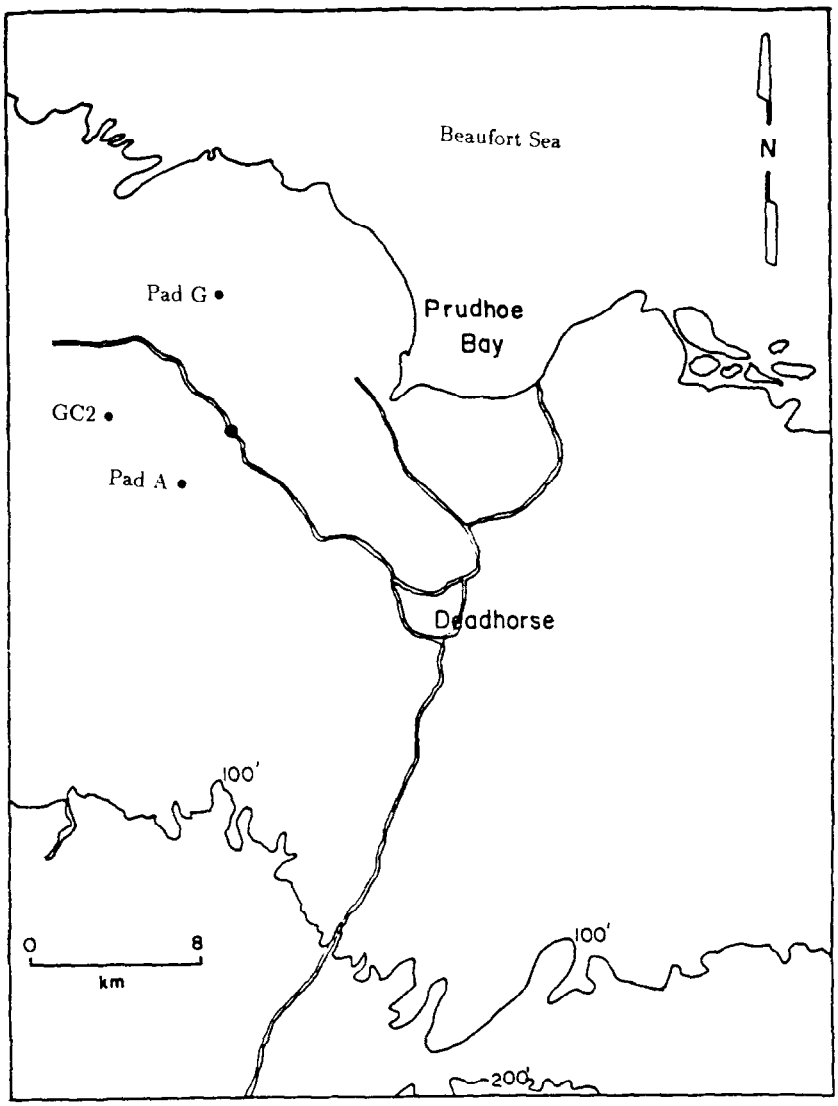

Fig. 1. Map of the Prudhoe Bay oilfield.

continuous basis with a Doppler acoustic sounder located at well pad A. Additional wind data were recorded on an instantaneous basis with two UVW (3 wind components – u, v, w) propeller anemometers. One instrument was mounted on a 3 m mast attached to a 30 m communications tower (a total of 33 m above the tundra surface) on the edge of an oil gathering center (GC2). This location was selected to provide measurements of the approach flow for our tracer investigations of dispersion near GC2. Analysis of the variation in turbulence with wind direction indicates that the tower and nearby buildings, which are about 20 m high and were downwind for the predominant winds, had a small influence on these measure-

ments. The second instrument was operated during tracer tests in a portable mode on a 2 m mast and moved periodically during tests to various locations downwind of the oil gathering center.

It should be noted that our study of the arctic ABL includes measurements within the wake of industrial facilities, discussed in our analysis of plume downwash and building-enhanced dispersion (Guenther *et al.*, 1989b), and the open terrain measurements described in this paper. The open terrain measurements are not significantly influenced by the immediate presence of buildings but they are representative of the boundary-layer flow over the widely scattered roads, pipelines, and industrial facilities of the oilfield reservation. Data completeness of 90% was achieved during this field study and the generally high quality of the data has been described by Guenther *et al.* (1988). The uncertainties associated with the observations reported in this paper are within reasonable limits and provide the assurance of data accuracy needed for characterizing an arctic ABL.

Figure 1 indicates the locations of the three sites used to investigate the arctic boundary layer: well pads A and G and an oil gathering center (GC2). The well pads consist of a series of low (10 m) buildings on one side of a large, raised (1 m) gravel pad. Well pad G provided an undisturbed approach flow with the predominant easterly winds (about a 5 km fetch). Instruments at heights of 11 and 17 m were located on the eastern edge of the well pad, about 50 m east of the well pad buildings. Instruments at heights of 1 and 3 m were located above the tundra on a tripod 90 m east of the well pad buildings. Aspirated thermistors (Climet model 015) measured temperature and cup anemometers (Climet model 011) recorded wind speed at all four levels. A pyranometer (Eppley Model 8-48) provided solar insolation at 1 m while wind direction was measured at 11 m (Climet model 012). A sampling frequency of 1 Hz and an averaging time of 15 min provided 900 samples per averaging period. Data were recorded with an IBM PC portable equipped with LABMASTER and Metrobyte DASH8 A/D cards.

Wind speed and direction data were obtained at well pad A using a Doppler acoustic sounder (AeroVironment model 2000) which was operated by the Alaska Department of Environmental Conservation. Doppler shifts in the back-scattered signals were sampled at a rate of 0.1 Hz and averaged over 15-min periods for 14 heights between 60 and 450 m (30 m windows). The well pad buildings located about 50 m to the east of the acoustic sounder should have had little impact on the flow at these heights. The presence of snow in the antennae dishes degraded the quality of measurements made October 23–26 and November 7–9 and these data were not included in our analysis of the arctic ABL. Gill UVW propeller anemometers provided measurements of the instantaneous velocity components near GC2. One anemometer was located on the northeast edge of the complex at a height of 33 m (13 m above the nearby buildings). A second UVW anemometer was used to record the flow near ground level (2 m) at various locations between 50 and 2300 m downwind of the gathering center complex. The output from both instruments were recorded at 1 Hz with micro-computer data systems.

Open terrain tracer data were collected during tracer tests 2 and 3 with light

west winds on the open tundra about 1 km west of GC2. An open terrain release was conducted during tracer test 8 with high east winds at a site about 1 km north of the gathering center. Sulfur hexafluoride (SF_6) tracer gas was released at a steady rate during these three tests from a height of 1 m above the tundra. SF_6 was released from a source within the oil gathering center during tracer tests 1 and 4–10. The results of these building-enhanced dispersion tests are described by Guenther *et al.* (1989b). During all ten tests, 1-hr averaged air samples were collected with portable syringe samplers deployed at positions ranging from 100 to 1000 m downwind. Samples were analyzed with portable electron capture gas detectors located in a field lab. The detection limit of this system is approximately 1 part per trillion (ppt).

3. Results and Discussion

3.1. Introduction

The variations in 15-min averages of insolation, temperature, wind speed, and wind direction collected at a height of 11 m at well pad G during the study are displayed in Figure 2. These conditions are typical of the Prudhoe Bay area and include periods of light ($<5\ m\ s^{-1}$) east or west winds with clear skies as well as moderate (5 to 10 $m\ s^{-1}$) east winds from October 23 to November 4 and a winter storm with $>10\ m\ s^{-1}$ winds and limited visibility due to blowing snow from November 5 to 9. Table I describes the four subsets of this time period which represent conditions typical of the study. Each subset includes a 7-hr period (0900 to 1600) on separate days. Our first data subset was collected on October 25 (tracer test 3) when steady, light west winds were accompanied by a stable ($2–6\ °C \cdot (100\ m)^{-1}$, temperature gradient from the surface to 10 m. As the light winds recorded during our second data subset on October 27 (tracer test 4) varied from northeast to southeast, the strength of the surface temperature inversion increased to $18\ °C \cdot (100\ m)^{-1}$). The third data subset, tracer test 6 (November 2), was characterized by higher wind speeds with the wind direction varying from northeast to north and a slight thermal stability (1 to $2\ °C \cdot (100\ m)^{-1}$) between 1 and 11 m. The strong steady east winds recorded in our fourth data subset recorded on November 5 (tracer test 8) were also accompanied by slight thermal stability below a height of 11 m. It should be noted that open terrain tracer data, described in this paper, were collected during tracer tests 3 and 8 whereas building-enhanced tracer data, described by Guenther *et al.* (1989), were collected during tracer tests 4, 6 and 8.

3.2. Surface layer structure and turbulence

Turbulence in the ABL is produced by mechanical and convective processes. Mechanically induced turbulence is a function of the surface roughness and wind speed. Convectively induced turbulence is generated when thermal instabilities produce vertical movements as a result of buoyancy forces. In the lower latitudes,

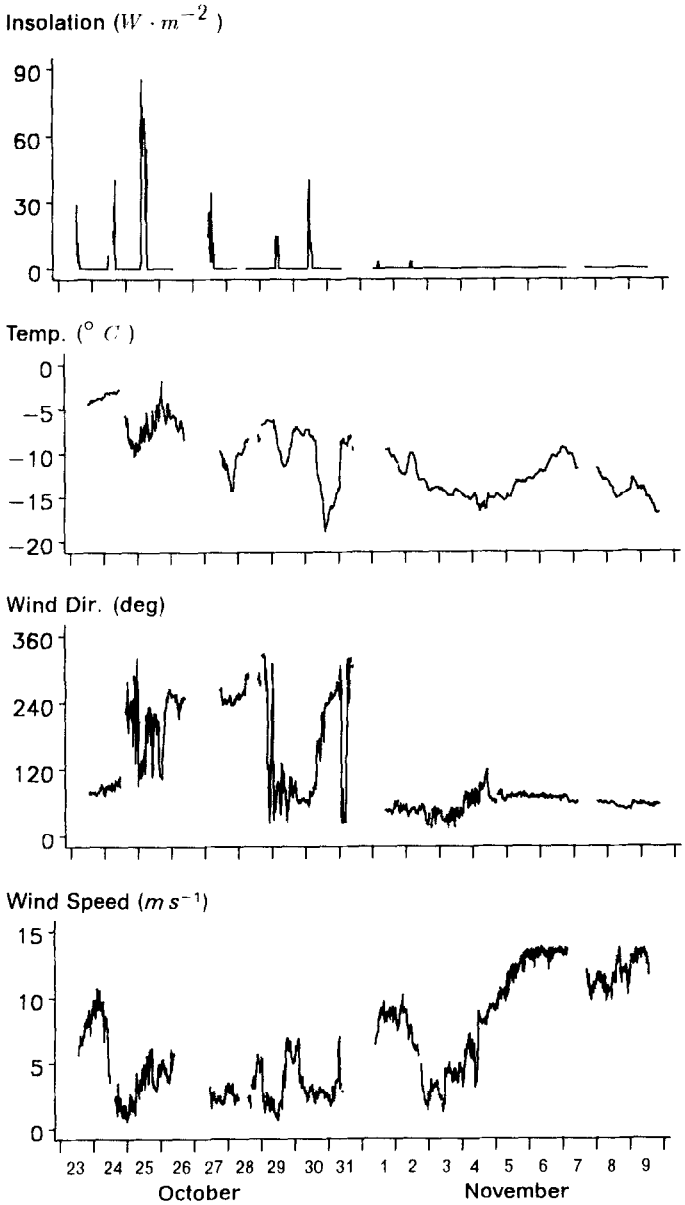

Fig. 2. 15-min averages of solar insolation, temperature, wind direction and wind speed at a height of 11 m at well pad G from October 23 to November 9.

daytime heating results in thermal instability, while nighttime cooling produces a thermally stable surface layer. High wind speeds are associated with near neutral thermal stability whereas low wind speeds are associated with a diurnal pattern of stability.

Using several vertical levels of wind speed to generate a logarithmic profile, Dalrymple *et al.* (1966) calculated a roughness length (z_0) of 0.014 cm in the frozen

TABLE I

Meteorological conditions typical of the field study

Test	3	4	6	8
Date	Oct. 25	Oct. 27	Nov. 2	Nov. 5
Wind speed at 33 m ($m \cdot s^{-1}$)	4–5	3–5	8–11	16–17
Wind Dir. at 33 m	steady NW	meandering NE–SE	meandering ENE–NNE	steady E
$\frac{\Delta T}{\Delta Z}$ from 1 to 11 m ($°C \cdot (100\,m)^{-1}$)	2–6	2–18	1–2	1–3
Other	Clear skies	overcast	blowing snow	blowing snow

Antarctic snow fields. Weller and Holmgren (1974) used the same method and found significant seasonal changes in z_0 that varied from 4.07 cm during the initial freeze-up of the arctic tundra near Barrow, Alaska, to 0.03 cm in mid-winter. We evaluated 471 logarithmic profiles of four levels of 15-min average wind speeds. These periods were selected on the basis of having a logarithmic increase in wind speed with height and of having a wind speed, at a height of 3 m, greater than 5 m s^{-1}. The z_0 calculated from these data is 0.03 cm for the open tundra east of well pad G in the Prudhoe Bay area during this study. The agreement of these estimates of z_0 suggests that our measurements are representative of other open tundra sites.

The limited solar insolation in the arctic from October to April does not provide the daytime heating necessary for a diurnal cycle of atmospheric stability. Weller and Holmgren (1974) have reported an average albedo of 85% for the arctic snowfields. Our measurements indicate that the average solar insolation was never more than 90 $W \cdot m^{-2}$ for any 15-min period of the study. The amount absorbed at the surface was therefore always less than 15 $W \cdot m^{-2}$ and usually much less than 1 $W \cdot m^{-2}$. In several cases, illustrated in Figure 3, surface air temperatures decreased, rather than increased, during periods of maximum solar insolation. The decrease in surface air temperature corresponds with a change in wind direction, from east to south, which replaced the relatively warm maritime air with a cold continental air mass. A comparison of hourly averaged $\Delta T/\Delta Z$ vs wind direction measured during the study is shown in Figure 4 and indicates that extremely stable conditions occurred more frequently with south and west (continental) winds. The vertical temperature gradients shown in Figure 5 indicate that although these strong positive temperature gradients occur only with wind speeds below 5 m s^{-1}, a slight thermal stability occurs even with high wind speeds above 10 m s^{-1} independent of wind direction.

Hanzlick *et al.* (1988) observed 10–20 km of open ocean between the coastal sea ice, which extended 10 km from shore, and the offshore pack ice in the

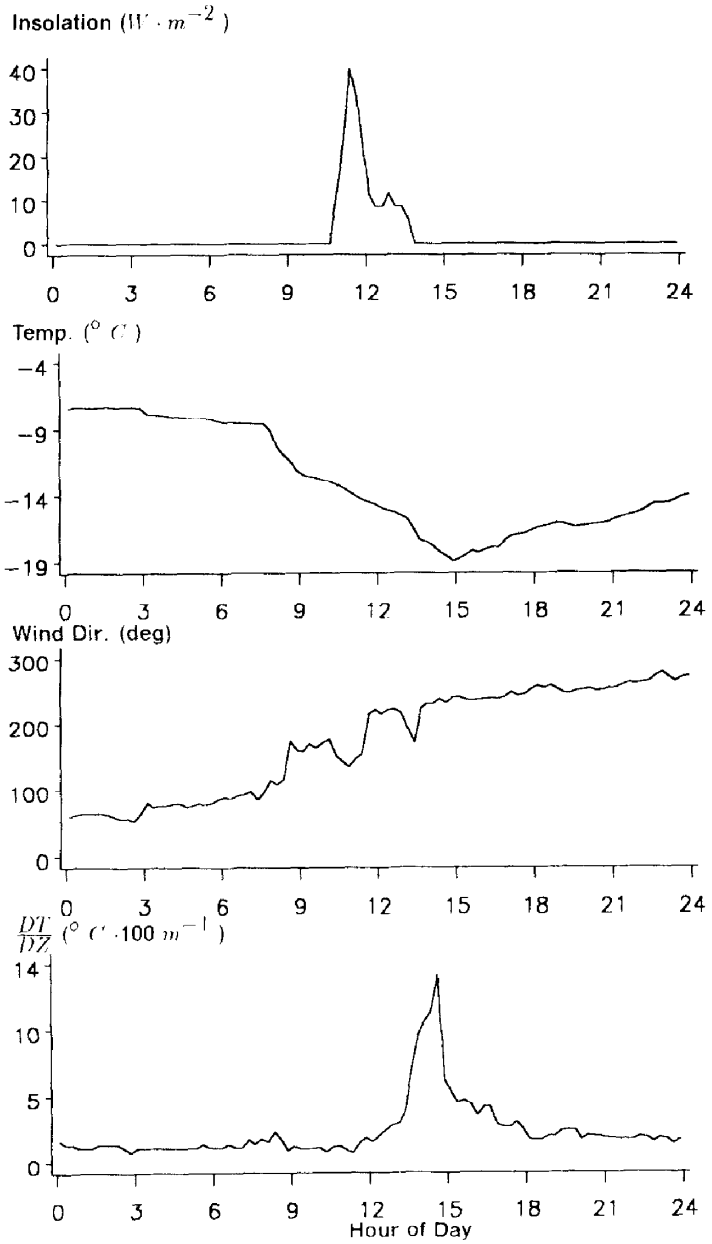

Fig. 3. 15-min averages of solar insolation, temperature and wind direction at a height of 11 m and the vertical temperature gradient between 1 and 11 m at well pad G on October 30.

Prudhoe Bay area during late October of 1987. The slightly stable surface layer which we observed in the Arctic even during high winds is a pattern which matches the classical description (Wexler, 1936) of the energy balance which occurs when an unstable polar marine air mass, generated by the surface of the relatively warm

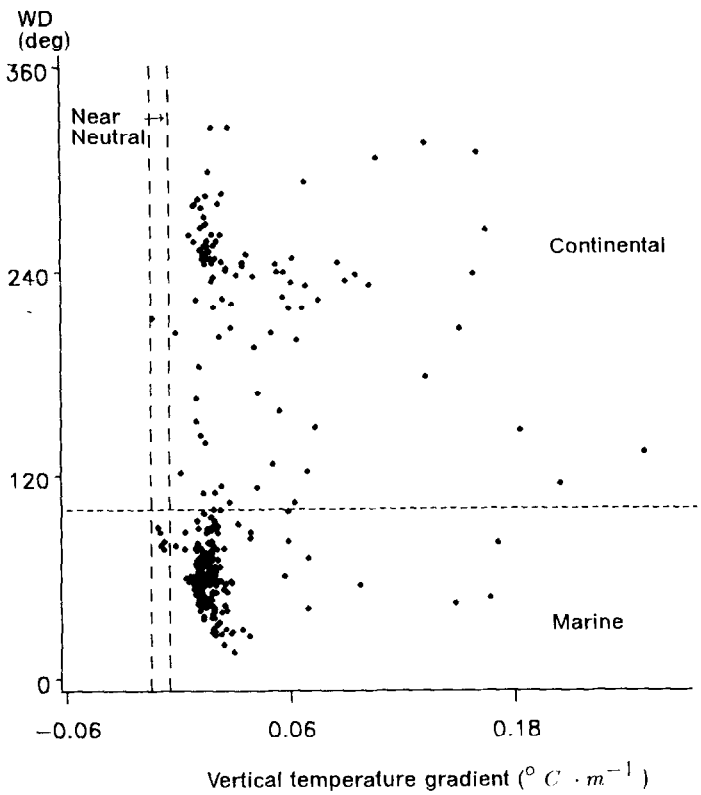

Fig. 4. Distribution of vertical temperature gradient between 1 and 11 m by wind direction (15-min averages) showing the influence of maritime and continental fetches.

ocean water, is transformed into a thermally stable continental air mass by the relatively cold tundra surface. Although the Beaufort Sea is completely frozen over by December, it is likely that this phenomena persists to some extent for the duration of the long arctic winter since the air over sea ice tends to be warmer than nearby continental snow cover (Wexler, 1936).

In comparison to typical diurnal patterns of atmospheric stability commonly incorporated into air quality models, the winter-time arctic boundary layer is quite different. In the Arctic, clear skies and light winds are associated with strong stable temperature gradients in the surface layer even during mid-day, whereas in other climates, strong stable temperature gradients are usually associated with nighttime clear sky periods. In non-arctic regions, strong winds typically imply neutral stability conditions throughout the surface layer. In polar regions, however, a shallow surface inversion continues to exist even with high winds. To investigate the temperature structure of the winter-time arctic ABL above 17 m, we analyzed 120 National Weather Service (NWS) soundings of temperature and wind speed between the surface and 10 km at Barter Island and Barrow, Alaska. When the

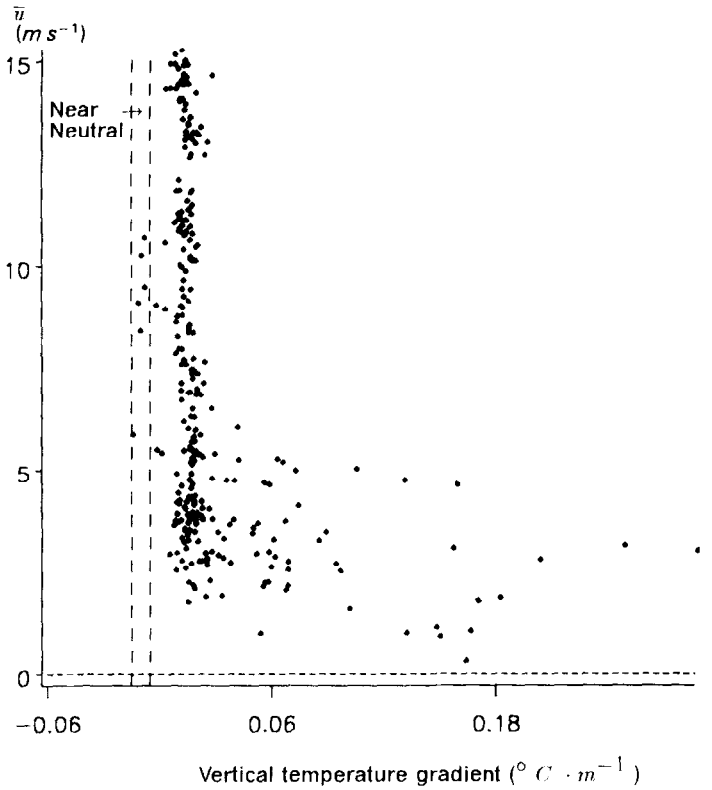

Fig. 5. Distribution of vertical temperature gradient by wind speed based upon 15-min averages recorded during the study.

surface winds were greater than 10 m s^{-1}, a near-neutral layer was almost always observed between approximately 15 and 300 m. An elevated inversion (2 to 5 °C · (100 m)$^{-1}$) was measured between 300 and 600 m in each high wind speed case. Dispersion from the short stacks (20 to 40 m) typical of arctic industrial facilities is primarily influenced by the neutral conditions observed between heights of 15 and 300 m during strong winds. The smooth snow-covered surface, which can be found in winter in the lower latitudes, may have an influence on the surface layer which should be incorporated into atmospheric dispersion models.

The effects of the smooth, snow-covered surface upon boundary-layer structure and turbulence can be examined in terms of the friction velocity u_*, the sensible heat flux H, and the scaling length for surface layer turbulence, the Monin–Obukhov length L:

$$L = -\frac{\rho C_p u_*^3 T}{kgH} \tag{1}$$

where ρ is the density of air, C_p is the specific heat constant for air, k is the von

Karman constant (=0.4), and g is the gravitational constant. We employed the method of Berkowicz and Prahm (1982) to derive these parameters from the 15-min averaged vertical profiles of wind speed and temperature at well pad G. In this approach, temperature and wind speed at 1 and 11 m were used with the Businger functions for non-dimensional wind speed and temperature in an iterative approach to solve for L, and then u_* and θ_* (the surface scaling velocity and temperature), and H. Given these terms, we also calculated the production rate of turbulent kinetic energy (TKE) due to wind shear ($S = u_*^3/kz$), where z is the height above ground, the production rate or dissipation of TKE due to buoyancy effects ($B = gH/\rho C_p$), and the rate of viscous dissipation of TKE ($\epsilon = S(\phi_m - z/L)$), where ϕ_m is the non-dimensional wind speed profile. Eddy diffusivities for heat and momentum were also obtained as $K_h = ku_*z/\phi_h$ and $K_m = ku_*z/\phi_m$.

The results of these calculations are given in Table II for the four representative periods described in Table I. During the clear-sky, light NW winds of test 3, the thermal stability was relatively strong, and the friction velocities were relatively small between 0.13 and 0.21 m s^{-1}. The Monin-Obukhov length ranged from 110 to 26 m and the surface heat flux was small. Turbulent production due to wind shear was modest between 10 and 35 cm^2 . s^{-3}, while buoyancy effects on TKE were small and negative. For test 4, where winds were also light and from the east, the temperature gradient was more stable and friction velocities were very low between 0.05 and 0.10 m s^{-1} . The Monin–Obukhov length ranged from only 4 to 23 m, and the surface heat flux was slightly negative. Shear production of

TABLE II

Stability and turbulence statistics based on hourly averaged wind speed and temperature measurements at heights of 1 and 11 m over snow-covered tundra

Test	Hour	U	WD	$\frac{\Delta T}{\Delta Z}$	Ri	u^*	θ^*	L	H	K_h	B	S	ϵ
3	1100	3.9	261	2.4	0.035	0.21	0.035	110	−10	0.69	−3	35	45
3	1200	3.0	244	5.6	0.101	0.13	0.050	26	−10	0.22	−3	10	20
3	1300	3.7	240	5.7	0.071	0.18	0.065	40	−17	0.38	−5	22	37
3	1400	3.3	245	3.7	0.068	0.15	0.043	43	−9	0.33	−2	11	19
4	0900	1.8	081	18.4	0.257	0.07	0.067	6	−6	0.03	−2	1	7
4	1100	1.2	045	15.9	1.24	0.05	0.045	4	−3	0.02	−1	1	3
4	1200	2.6	072	7.4	0.130	0.10	0.051	16	−8	0.12	−2	5	12
5	1400	2.3	081	1.7	0.101	0.07	0.015	23	−1	0.10	−1	1	2
6	0900	9.0	050	1.2	0.008	0.38	0.022	486	−11	1.61	−3	168	179
6	1100	9.0	055	1.3	0.008	0.40	0.024	501	−13	1.70	−4	199	209
6	1300	7.7	044	1.4	0.015	0.28	0.024	260	−9	1.11	−3	73	81
6	1500	7.2	021	2.6	0.048	0.18	0.035	68	−8	0.48	−2	18	26
8	0900	14.0	075	1.5	0.004	0.64	0.028	1120	−24	2.90	−7	835	858
8	1100	14.3	074	1.6	0.004	0.64	0.029	1080	−25	2.89	−7	824	848

Wind speed, U (m · s^{-1}), and wind direction, WD (deg), were measured at a height of 11 m. The gradient Richardson number, Ri, vertical temperature gradient, $\Delta T/\Delta Z$ (°C · (100 m)$^{-1}$), friction velocity, u_* (m · s^{-1}), a temperature scale θ_* (°C), Monin-Obukhov length, L (m), heat flux, H (W · m^{-2}), eddy conductivity, K_h (m^2 · s), buoyancy dissipation of κ, B (cm^2 · s^{-4}), shear production of κ, S (cm^2 · s^{-3}), and eddy dissipation of κ, ϵ (cm^2 · s^{-3}) are based on measurements at 1 and 11 m.

TKE was much smaller for test 4 than for test 3. The difference may be associated with slightly lower wind speeds in test 4 than in test 3 and also with test 3 being carried out for northwest winds which may have a greater surface roughness due to the proximity of the gravel well pad and pad structures than for test 4 with east winds where the fetch was completely open tundra.

For tests 6 and 8, with strong winds exceeding 8 m s^{-1} the temperature gradient was less positive, and friction velocities of 0.18 to 0.64 m s^{-1} were significantly larger than for the light wind tests. Similarly, the Monin-Obukhov length was also larger in the range 68 to 1120 m, indicating more neutral conditions. As we would expect, the shear production of TKE was also large compared with that in the light wind tests. The effects of this shear production are evident in the eddy diffusivities given in Table II. For light winds, K_h was generally much less than one whereas for strong winds K_h was in the range 0.5 to 2.9 m^2 s^{-1}. These values suggest that the strong winds are effective at producing relatively large diffusion rates in spite of the smooth surface and the presence of the surface temperature inversion.

3.3. Moments, stresses, and spectra of velocity components

From the preceding discussion, we have seen that the arctic boundary layer contains a shallow surface inversion with a strength dependent upon wind speed, and that the turbulence in this layer is generated by wind speed shear. We can look further into the characteristics of the arctic turbulent boundary layer by examining the statistics of instantaneous velocity fluctuations measured near the surface. We recorded instantaneous 3-component wind speeds with two UVW anemometers during tracer release periods each lasting from 3 to 8 hr in duration. For both systems, the data were reduced by rotating the coordinates to yield, for 5-min periods, U equal to the mean wind speed along the mean wind direction and $V = W = 0$. In this discussion, we examine primarily the results from the 33 m tower near GC2. Although the data collected with this system may reflect the wake effects of nearby (lower) buildings, the low wind velocity variances measured at 33 m indicate that any building effects are minimal.

Statistical parameters from the 33 m wind data are given in Table III for the four periods described previously. For these periods, the third and fourth moments of all three velocity components, calculated for 5-min periods, yield a skewness near 0 (± 0.3) and a kurtosis of 3 (± 0.5), which agree with the expected Gaussian nature of small-scale turbulence. The hourly average turbulent intensities exhibited only small differences between the light wind and the strong wind situations. Although both longitudinal and horizontal crosswind intensities had a minimum of 4%, longitudinal intensities ranged up to 9% while the maximum horizontal intensity was about 7%. Vertical turbulent intensity was smaller in the range of 2 to 5%. Friction velocities calculated from the instantaneous velocity fluctuations at 33 m near GC2 agreed within 20% of most of the values derived from the mean profile data at 11 m on well pad G. The average value of $u_*/\bar{u}$ measured during this study was 0.030 which is similar to values reported in the literature (Deacon,

1973). The ratios of standard deviations of wind velocity components to u_* is usually nearly constant in the surface layer, but are a function of atmospheric stability and surface roughness. Panofsky and Dutton (1984) have compiled values from a number of studies conducted in flat terrain and report averages of $\sigma_w/u_* = 1.25$, $\sigma_v/u_* = 1.92$, and $\sigma_u/u_* = 2.39$ for neutral conditions. Results specific for snow-covered surfaces are not available. These ratios increase with increasing stability so that our observed average values during the study of $\sigma_v/u_* = 1.92$ and $\sigma_u/u_* = 2.54$ are comparable. Our average for σ_w/u_* of 1.15 is slightly less than the typical value for neutral conditions.

Total turbulent kinetic energy per unit mass ranged from 0.04 to 0.12 $m^2 \cdot s^{-2}$ for the low wind speed tests, but increased to between 0.3 and 2.1 $m^2 \cdot s^{-2}$ for the high wind speed tests. This gives an overall measure of the turbulent stresses and agrees with the profile-based results showing increased production of TKE due to wind shear for higher wind speeds.

The total lateral wind direction standard deviation ($\sigma_{\theta T}$) for 1-hr periods was in the range 3 to 7° for the high wind tests, and increased to between 3 and 15° for the low wind tests. We can examine the contributions of low frequency meander versus the contributions of high frequency fluctuations in terms of the hourly standard deviation of 5-min average wind direction ($\sigma_{\theta l}$) and the hourly average

TABLE III

Turbulence statistics based on three-component (u, v, w) wind speed measurements at a height of 33 m on the upwind edge of an oil gathering center

Test	Hour	U	WD	$\sigma_{\theta T}$	$\sigma_{\theta h}$	$\sigma_{\theta l}$	$u*$	κ	$\frac{\sigma_u}{U}$	$\frac{\sigma_v}{U}$	$\frac{\sigma_w}{U}$
3	1100	4.3	291	3.5	2.4	2.6	0.11	0.04	4.4	4.2	3.0
3	1200	4.2	296	5.4	3.0	4.4	0.15	0.11	7.7	5.2	4.5
3	1300	4.8	297	3.6	3.2	1.5	0.18	0.11	7.7	5.4	5.0
3	1400	4.7	295	4.0	3.1	2.5	0.19	0.12	7.5	5.3	4.6
4	0900	3.3	103	5.3	2.5	4.7	0.06	0.04	6.1	4.4	2.3
4	1100	3.0	073	7.6	4.1	6.4	0.08	0.04	5.8	7.2	2.8
4	1200	4.5	085	14.8	2.7	14.5	0.08	0.07	5.8	4.8	1.8
4	1400	4.1	094	5.8	3.3	4.8	0.11	0.11	9.1	5.7	3.4
6	0900	10.5	050	5.1	3.3	3.9	0.29	0.47	6.5	5.6	3.0
6	1100	9.5	060	5.5	3.3	4.4	0.26	0.38	6.3	5.8	3.0
6	1300	8.4	044	6.7	3.0	6.0	0.25	0.29	6.4	5.2	2.9
6	1500	8.3	019	3.2	2.7	1.7	0.25	0.26	6.3	4.8	3.1
8	0900	16.2	087	4.3	3.6	2.3	0.55	1.74	9.1	6.1	3.6
8	1100	16.1	084	4.5	3.6	2.7	0.56	1.83	9.2	6.3	3.8
8	1300	17.1	084	5.0	3.4	3.7	0.61	2.12	9.7	5.8	3.5
8	1500	17.0	080	4.0	3.8	1.3	0.58	1.94	8.8	6.7	3.5

Wind speed, U ($m \cdot s^{-1}$), and wind direction, WD (deg), are hourly averages. The standard deviation of horizontal wind direction fluctuations is shown for 1-hr periods. ($\sigma_{\theta T}$), the hourly average of the standard deviation in 12 5-min periods ($\sigma_{\theta h}$) and the standard deviation of 12 5-min average wind directions ($\sigma_{\theta l}$). Friction velocity, u_*, ($m \cdot s^{-1}$), turbulent kinetic energy per unit mass, κ, ($m^2 \cdot s^{-2}$), and turbulent intensities, σ_u/U, σ_v/U and σ_w/U (%) represent the averages of 12 5-min periods. Coordinate rotations were applied to each 5-min period to yield U along the downwind axis and mean crosswind and vertical velocities of 0.

of 5-min standard deviations of wind direction fluctuations ($\sigma_{\theta h}$). As indicated in Table III, during low wind speed conditions, the low frequency changes in wind direction varied from 1.5 to 14.5° while the high frequency standard deviation ranged from 2.4 to 4.1° . A much greater range for the low frequency component (1.3 to 6.0°) than for the high frequency component (2.7 to 3.8°) is also evident for the high wind speed cases. Although very large low frequency contributions occurred only during low wind speeds (e.g., $\sigma_{\theta l}$ was a factor of 5 greater than $\sigma_{\theta h}$ during hour 12 of test 4), the low frequency component ranged from a factor of two greater to a factor of two less than the high frequency component for both low and high wind speed cases.

Standard deviations of hourly average wind direction measured at well pad G at 11 m were generally about a factor of 2 greater than those calculated from the data at 33 m at GC2. With the 25% reduction in velocity observed at 11 m compared with 33 m, the turbulent intensities were about 1.6 times larger at 11 m than at 33 m.

The distribution of wind speed variance provided by spectral analysis is frequently used to study TKE in boundary layers. Peaks in the spectra correspond to the production of TKE while gaps suggest dissipation or a lack of production. The spectra of the three wind-speed components displayed in Figure 6 are typical of the UVW anemometer data collected during the study. The spectral curves have been smoothed with a triangular weighting function which provides 20 deg of freedom and 90% confidence limits with a factor of 1.57 (Vinnichenko *et al.*, 1980). A 57% increase is small on the logarithmic scale used to display these spectra. Peaks in the spectra at a frequency near 0.1 Hz are associated with mechanically produced turbulence. The very low surface roughness in the Prudhoe Bay region contributes to the relatively low level of energy in the high frequency peaks observed for these spectra. As the wind speed increased from 3 m s^{-1} (Figure 6a) to 9 m s^{-1} (Figure 6b), the peak energy, nS(n), increased by a factor of 2 to 4 for all three wind components. The increased turbulence which we observed with higher wind speed has been observed in other boundary layers (Lumley and Panofsky, 1964). A decrease in elevation from 33 m (Figure 6b) to 2 m (Figure 6c) resulted in about a factor of 2 increase in peak energy for all three components. This increase is expected (Kaimal *et al.*, 1982) and is a result of the mechanical production of turbulence at the surface by frictional forces.

Convective eddies which result from thermal instabilities are generally larger than mechanically produced eddies. Their size is proportional to the height of the mixing layer. Kaimal *et al.* (1982) found that spectral energy at frequencies corresponding to these dimensions (0.01 to 0.001 Hz) is strongly dependent on thermal stability. Unstable, convective conditions result in a large peak in this region whereas a stable ABL leaves an energy gap. Figure 6a demonstrates an energy gap characteristic of the spectra we observed during light winds and $\Delta T/\Delta Z > 3°\,\mathrm{C} \cdot (100\,\mathrm{m})^{-1}$. The flattened spectral curve in Figure 6b is characteristic of our measurements made during strong east winds and indicates neutral or slightly stable conditions.

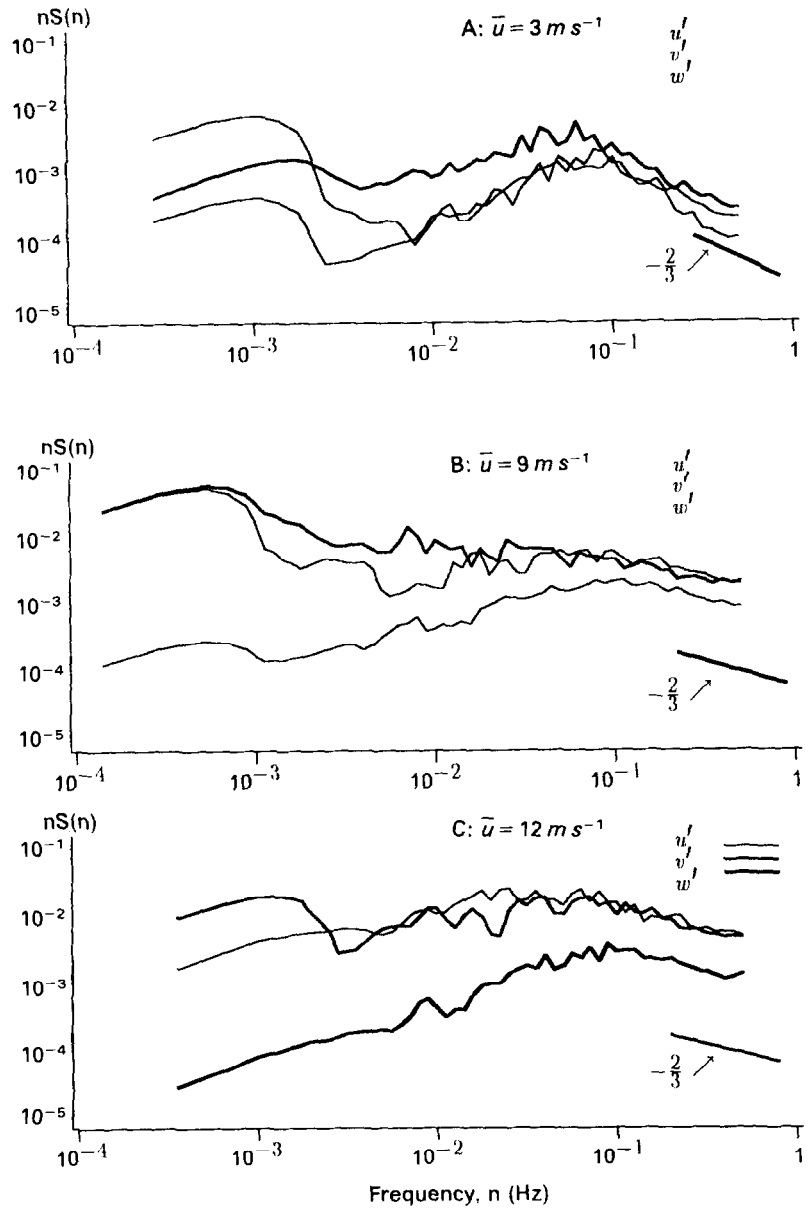

Fig. 6. Logarithmic spectra of wind speed components for light winds at 11 m (A), strong winds at 33 m (B) and strong winds at 2 m (C). Spectra are based upon UVW anemometer measurements with a 45-min to 1-hr sampling time and a 1-Hz sampling frequency.

Kaimal *et al.* (1972) have described the behavior of TKE spectra which were collected in the surface layer of the atmosphere on the plains of the midwestern United States. By normalizing with shear stress, u_*^2, the spectra collapse to a set of curves, depending on atmospheric stability, which converge to a single curve in the inertial subrange. Figure 7 demonstrates that the spectra we observed in

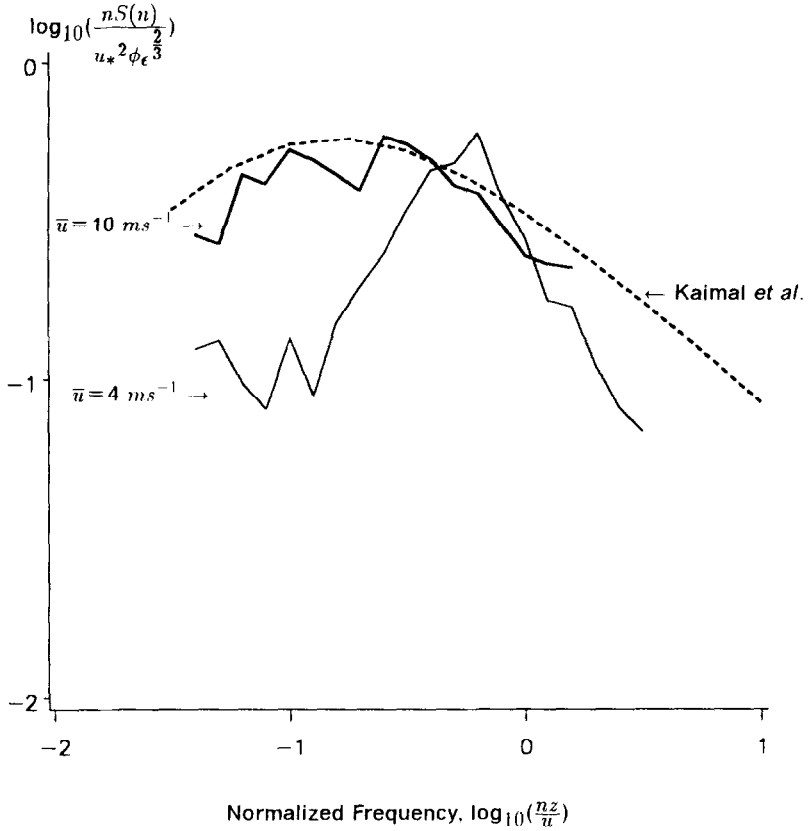

Fig. 7. Normalized logarithmic u spectra measured at 33 m near GC2 compared to Kaimal *et al.* (1972) (dashed line).

the arctic ABL also converge in the inertial subrange and are similar in shape and magnitude to those reported by Kaimal *et al.* when normalized by u_*^2 and the normalized eddy dissipation rate $\phi_\epsilon = \epsilon kz/u_*^3$. Our spectra tend to have a constant slope of $\sim -2/3$ at frequencies above 0.1 Hz which indicates that this region is within the inertial subrange, where energy is transferred to and dissipated at microscales, which provides the basis for applying Kolmogorov's inertial subrange law to estimate ϵ:

$$\kappa S(\kappa) = C\epsilon^{2/3}\kappa^{-2/3} \tag{2a}$$

where $S(\kappa)$ is the TKE at wavenumber κ and C is a dimensionless constant. Taylor's hypothesis that the wavelength $\lambda(=\kappa/2\pi)$ is equal to the ratio of mean wind speed, U, and frequency, n, allows us to rearrange this equation to provide a relationship for fixed-point frequency spectra:

$$nS(n) = \alpha U^{2/3}\epsilon^{2/3}n^{-2/3} \tag{2b}$$

where $\alpha = C/2\pi^{2/3}$. Using the values of α suggested by Pasquill and Smith (1983) (0.15 for the streamwise velocity component and 0.2 for the crosswind and vertical components), estimates of ϵ from our observed spectra range from 0.1 to 3 $cm^2 \cdot s^{-3}$. Estimates of ϕ_ϵ, which would be 1 for neutral conditions, range from 0.05 to 0.5 indicating that our measured eddy dissipation is lower than what is expected ($\epsilon = u_*^3/kz$) for the high wind speeds we observed. Although our use of UVW anemometers and a relatively slow sampling rate (1 Hz) are not ideal for investigating these very small scales of turbulence, the data do provide an indication of the structure of turbulence in the winter-time arctic boundary layer.

Spectral peaks at lower frequencies ($<1 \times 10^{-3}$ Hz) were highly variable but often made significant contributions to the total TKE. Representative spectra of the crosswind fluctuations at frequencies less than 1×10^{-3} Hz obtained from wind direction and cup anemometer data are shown in Figure 8. With high wind speeds, a peak in TKE was associated with frequencies near 7×10^{-5} Hz (a time scale of about 4 hr). Moderate wind speeds had a secondary peak near 3×10^{-4} Hz (a time scale of 45 min). Low wind speeds had a relatively much larger TKE which decreased with decreasing frequency.

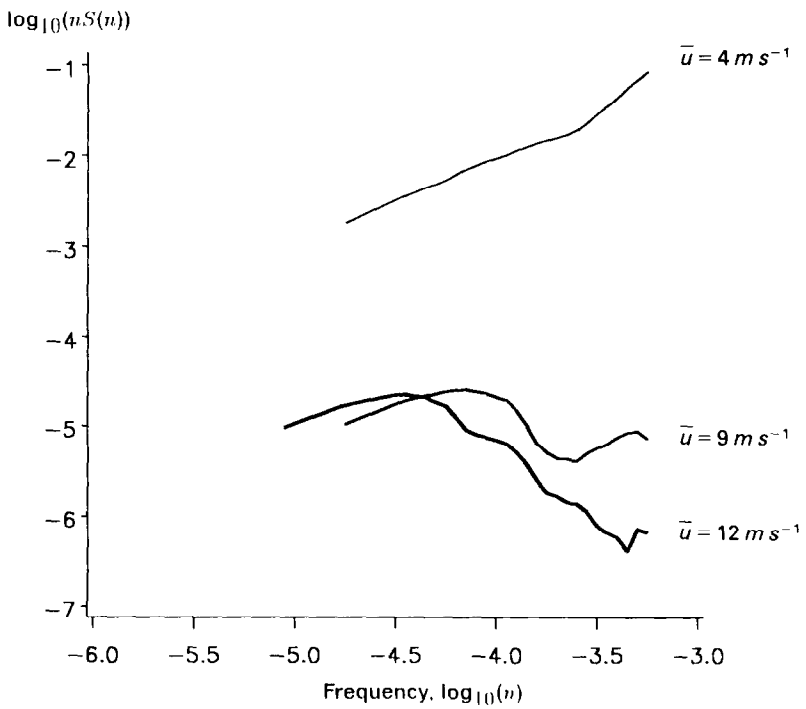

Fig. 8. Logarithmic crosswind spectra for a height of 11 m at low frequencies for light, moderate and high wind speeds.

3.4. Wind profiles and diffusion coefficients

Air quality models based upon the Gaussian plume equation require estimates of wind speed and diffusion parameters. Wind speeds at various heights in the ABL can be extrapolated from a single reference height using a power law relationship:

$$\frac{u_{z2}}{u_{z1}} = \left(\frac{z_2}{z_1}\right)^p \tag{3}$$

where u_{z2} is the wind speed at some height, z_2, u_{z1} is the wind speed at a reference height z_1 and p is a power law coefficient. A value of ~1/7 is usually used for p in a neutral boundary layer. Irwin (1979) reports p as a function of both z_0 and atmospheric stability. With $z_0 < 0.01$ m, Irwin's estimates suggest $p < 0.06$ during unstable conditions and $p > 0.34$ during stable conditions. Best fit estimates of p for 4 levels of wind speed at heights of 1 to 17 m collected throughout the study ranged from 0.2 to 0.35 during stable conditions and were between 0.06 and 0.14 during slightly stable or neutral conditions. These values are less than the default values in current regulatory dispersion models.

The vertical profiles of wind speed and direction between 60 and 450 m shown in Figure 9 were measured with a Doppler acoustic sounder during low and high wind speeds. An exponential increase in wind speed with height and a relatively low wind shear due to variation in wind direction with height were typical of most high (curve C) and moderate (curve A) easterly surface winds. As surface winds shifted from easterly maritime flow to westerly continental flow between 0600 and 0900 hr of October 30 (curves A and B in Figure 9) an extremely stable surface layer ($>5\ ^\circ\text{C} \cdot (100\ \text{m})^{-1}$) was measured near the ground and a shear layer at 200 m was evident in both the wind speed and direction profiles.

Gaussian diffusion coefficients, σ_y and σ_z, can be estimated using direct measurements of turbulence or using the various methods which categorize the ABL into a small number of discrete stability classes based on mean meteorological observations. The variation in the Pasquill–Gifford (PG) stability category predicted by four separate methods during a 10-hr period is illustrated in Figure 10. The vertical temperature gradient, $\Delta T/\Delta Z$, predicts extreme stability (class F or G) while methods based on both temperature and wind speed profiles (L and Ri) predict neutral or slight stability (class D or E). The standard deviation of wind direction for 15-min periods also indicates neutral or slightly stable conditions.

The fact that different stability parameters indicate different stability conditions is not unique to the arctic. Sedefian and Bennett (1980) compared a number of stability parameters for tower measurements from a New York site and found similar differences. In terms of diffusion model applications, parameters such as Richardson number which incorporate both thermal and mechanical effects upon turbulence are the best measures of the degree of stability affecting plume diffusion.

In order to examine the effects of the arctic boundary layer on plume diffusion,

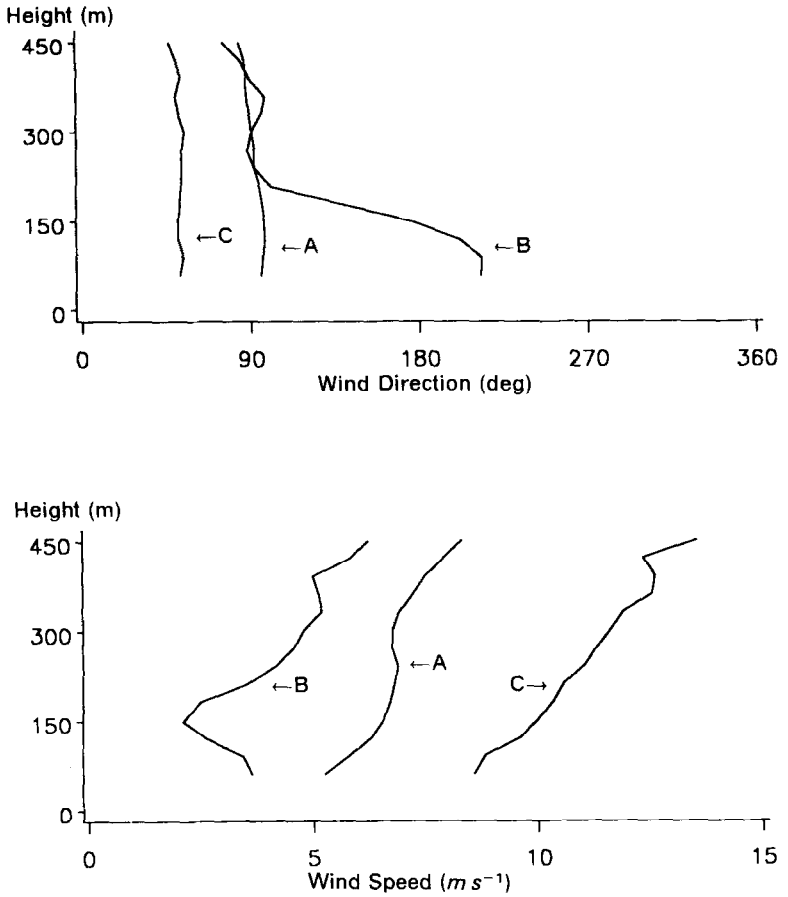

Fig. 9. Doppler acoustic sounder measurements of wind speed and direction at heights between 60 and 450 m at well pad A. Hourly averages shown are for 0600–0700 (curve A) and 0900–1000 (curve B) on October 30 and 0800–0900 on November (curve C).

different methods of calculation, especially for the low wind speed, extreme stability case.

concentrations were determined from over 500 samples collected during 17 1-hr periods over three different days including two days with light winds and one day with strong winds.

Examples of the data collected during low and high wind speeds are shown in Figure 11. The horizontal Gaussian diffusion coefficient σ_y was calculated from these data by using a nonlinear best-fit procedure. Although this method provides a good fit for short averaging times, hourly average concentration data often display a non-Gaussian distribution, which is the result of plume meandering. Neither the nonlinear best-fit method nor any other method, such as the crosswind profile integration described by Hanna (1986), can provide an appropriate estimate of σ_y when the concentration pattern deviates significantly from a Gaussian distri-

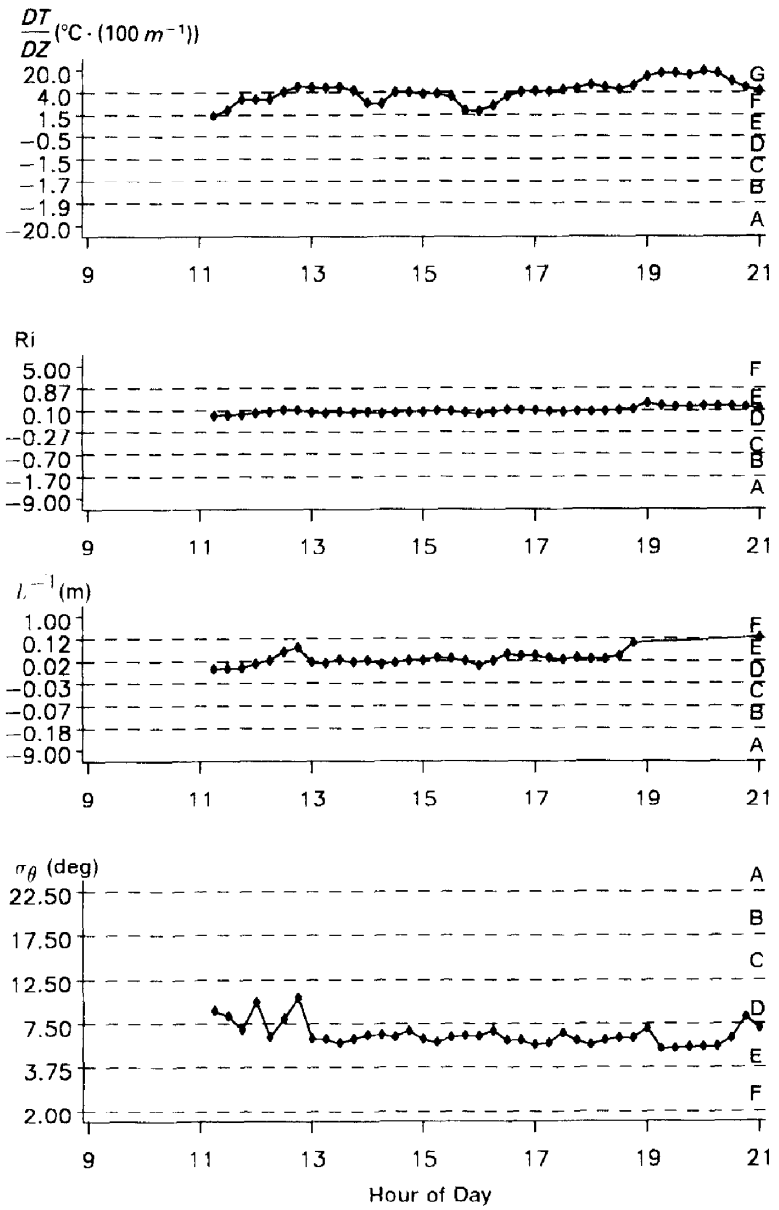

Fig. 10. Standard deviation of horizontal wind direction (σ_θ), vertical temperature gradient ($\Delta T/\Delta Z$), inverse Monin–Obukhov length (L^{-1}), and gradient Richardson number (Ri) estimated for 15-min periods with a 1-Hz sampling rate on October 23. Pasquill–Gifford stability categories are indicated for reference.

bution. Estimates of σ_y estimated by applying the best-fit procedure to our tracer data are depicted in Figure 12 relative to the PG stability curves. The observed horizontal diffusion coefficients exhibit considerable scatter and encompass a range of PG diffusion curves from near neutral to very unstable conditions. It is import-

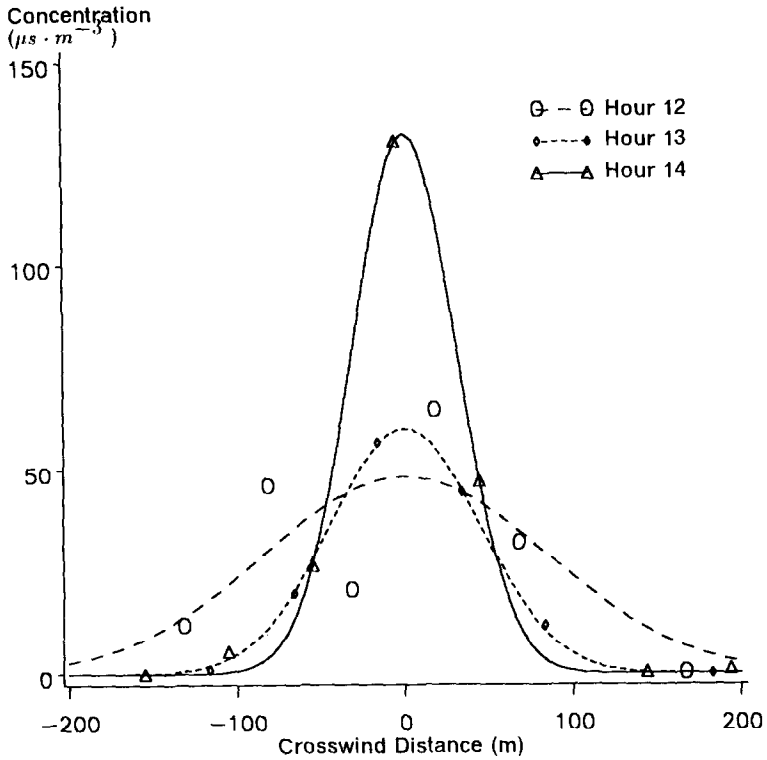

Fig. 11. Observed hourly averaged SF6 concentrations at 300 m downwind of open terrain ground releases during hours 12 (○), 13 (△) and 14 (◇) of test 8. Lines indicate best-fit Gaussian curves.

ant to note that in spite of the slightly stable to very stable atmospheric conditions, the observed horizontal diffusion rates range from one to several classes less stable than the atmospheric conditions warrant. To a certain extent, this difference can be attributed to the differences in averaging times between the hourly averaged observed data and the 3 to 10 min averaging times associated with the PG curves. For longer averaging times, increased wind meander will produce increased diffusion coefficients. From a diffusion modeling standpoint, however, hourly average concentrations are the primary concern so that using the PG curves immediately builds in a very conservative approximation to reality as evident in Figure 12.

The scatter in the diffusion coefficients is generally caused by forcing a Gaussian fit to non-Gaussian profiles. For example, Figure 11 shows that of the three high wind speed cases, hour 12, the large outlier high wind case (Δ) in Figure 12, has an hourly concentration profile that is bimodal with two equal sized maxima. The remaining two points for high winds represent concentration profiles with single maxima and Gaussian-like shapes. Occurrence of non-Gaussian profiles in the hourly data are associated with wind direction shifts or meander during the hour. Short-term (5-min) wind direction distributions, such as the high wind speed

examples shown in Figure 13a, were Gaussian for all test hours regardless of wind speed or σ_θ. The long term (1-hr) distributions were Gaussian in some cases and not in others. Figure 13b demonstrates that hour 12, which has a non-Gaussian plume profile (Figure 11) also has a non-Gaussian wind direction distribution. This indicates the impact that plume meandering can have on long-term plume profiles. From a modeling perspective, it will be necessary to model these situations in terms of sequential short-term (e.g., 5 min) periods and construct hourly profiles by averaging the short-term results. A typical Gaussian plume model with PG curves and hourly average meteorological data will not fare well in comparison with observed hourly data for these conditions.

Taylor's statistical theory of plume growth suggests that σ_y and σ_z should be proportional to σ_v and σ_w, respectively. Our estimates of σ_y from tracer data are plotted in Figure 14 vs $\sigma_\theta x (\approx \sigma_v t)$. These data indicate that the hourly σ_y does increase with hourly $\sigma_\theta (= \sqrt{\sigma_{\theta l}^2 + \sigma_{\theta h}^2}$, where the low frequency component, $\sigma_{\theta l}$, is the hourly standard deviation of four 15-min values of θ, and the high frequency component, $\sigma_{\theta h}$, is the hourly average of four 15-min σ_θ) although the ratio between the two is generally less than one. Taylor also showed that σ_y for travel

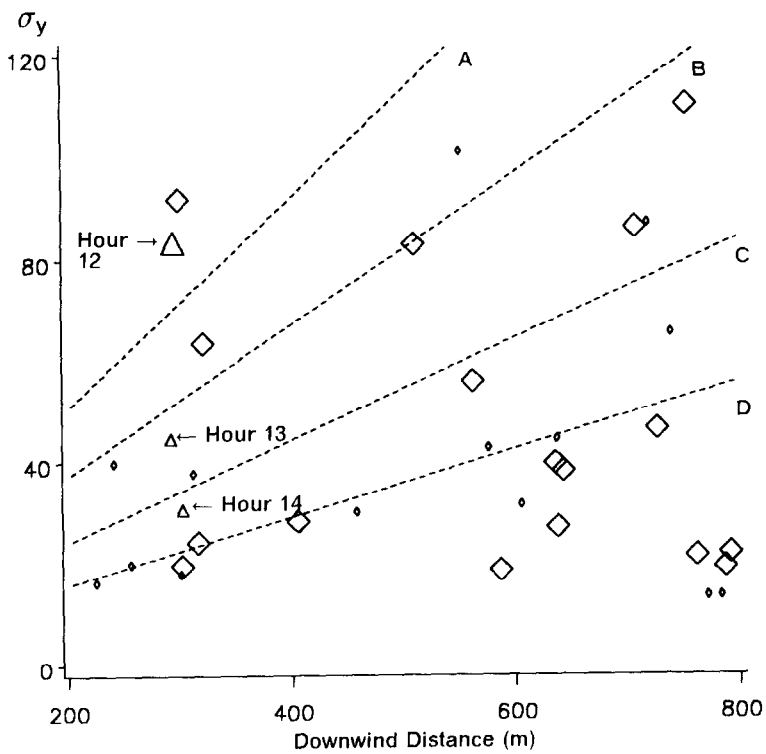

Fig. 12. Best-fit horizontal Gaussian dispersion coefficients, σ_y (m), from observed tracer distributions on the open tundra. Pasquill–Gifford curves are shown for reference.

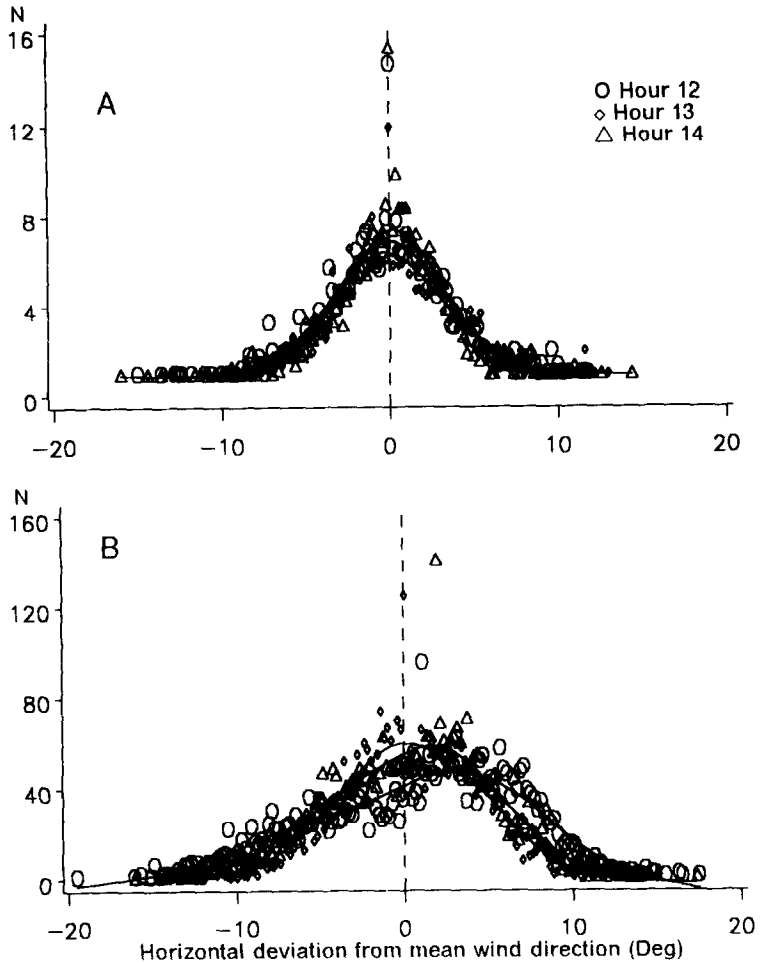

Fig. 13. Number of wind direction measurements (1 Hz) at a height of 33 m within 0.2° intervals relative to mean wind direction. The hourly mean of 5-min distributions (A) and the hourly distribution (B) are shown for hours 12 (○), 13 (△), and 14 (◇) of test 8.

times much greater than $2\tau_L$ (the Lagrangian time scale) increases at a rate proportional to $t^{0.5}$ rather than to t. We estimated τ_L by defining the Eulerian diffusion time scale, τ_E, as the time lag required to produce an autocorrelation of e^{-1} ($=0.3679$) and then estimated $\tau_L = (0.68/i)\tau_E$ (where i is the turbulence intensity, σ_v/U) as suggested by Pasquill and Smith (1983). Horizontal Lagrangian diffusion time scales calculated from UVW anemometer observations at 2 m ranged from 8 to 25 s while vertical τ_L ranged from 7 to 14 s. According to Taylor's theory, this suggests that the increase in σ_y will be proportional to the travel time for at least up to 10 to 25 s (50 m to 125 m downwind with a 5 m s^{-1} wind speed) and should be proportional to $\sqrt{t}$ at longer travel times (>50 s = 250 m downwind with a 5 m s^{-1} wind speed). The underestimation of σ_y by $\sigma_\theta x$ seen in Figure 14

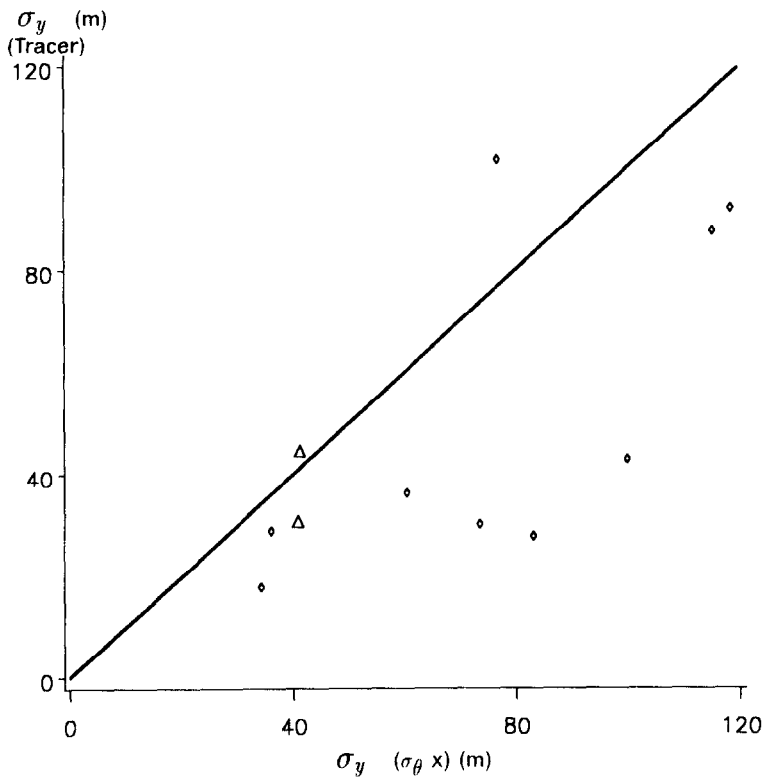

Fig. 14. Best-fit horizontal Gaussian dispersion coefficients, σ_y (m), from observed tracer distributions on the open tundra vs σ_v (m) estimated as $\sigma_v = \sigma_\theta x$.

for longer travel times (the larger values of σ_y) can be corrected somewhat with an equation that allows σ_y to increase proportional to $\sqrt{t}$ at longer travel times (e.g., Draxler, 1976)

The estimated vertical plume diffusion coefficients (σ_z) shown in Figure 15, calculated using a mass balance approach, exhibit considerable scatter due to their sensitivity to estimates of σ_y. Values which had a Gaussian crosswind plume profile (see Figure 15) indicate a stability ranging from neutral (PG class D) to stable (PG class F) atmospheric conditions. This is in agreement with the measured values of L and Ri. Figure 16 demonstrates that whereas there is a positive correlation between vertical (σ_w) and horizontal (σ_v) wind speed fluctuations, there is considerable scatter and also a factor of 5 range in hourly σ_v observed for specific values of hourly σ_w. A high σ_v and low σ_w are often observed with extreme stability, low wind speeds and significant meandering (a large $\sigma_{\theta l}$). A comparison of σ_v and σ_w for 5-min periods is also shown in Figure 16 and demonstrates that there is also a significant variation (factor of 3) in the small-scale horizontal turbulence for a given value of σ_w. This difference in vertical and horizontal turbulence suggests that vertical and horizontal plume diffusion require

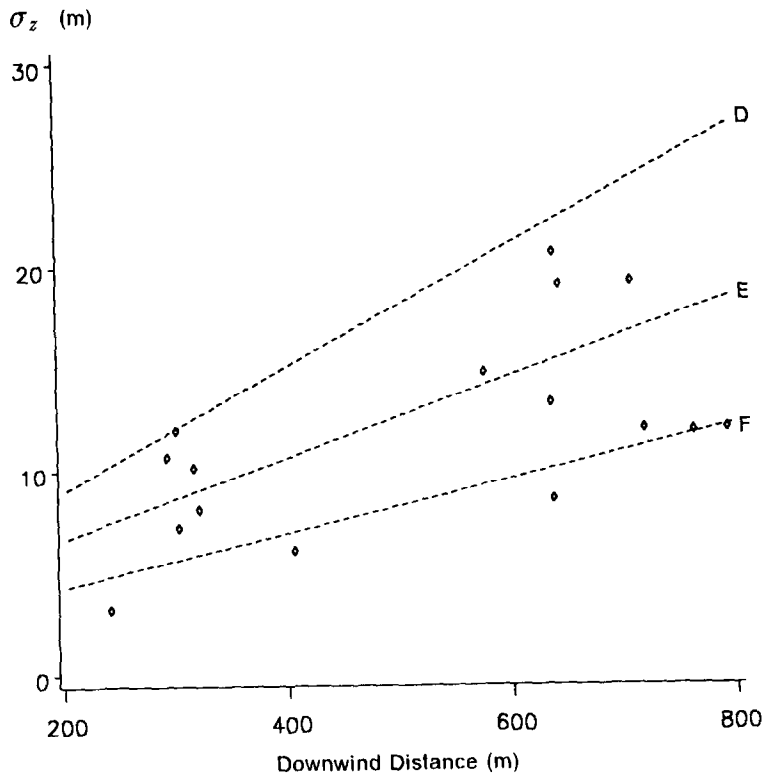

Fig. 15. Best-fit vertical Gaussian dispersion coefficients, σ_z (m), from observed tracer distributions on the open tundra. Pasquill–Gifford curves are shown for reference.

different methods of calculation, especially for the low wind speed, extreme stability case.

4. Summary and Recommendations

Our winter-time arctic micrometeorological measurements indicate that boundary-layer structure in the Prudhoe Bay region is influenced by the very smooth tundra surface, the limited solar insolation, and the nearby Beaufort Sea. The observed small surface roughness (0.03 cm) and persistent shallow surface inversion ($>1°\,C \cdot (100\,m)^{-1}$), which result from these influences are typical of other polar regions in winter but deviate from what is expected in the lower latitudes. In other ways, the structure of the arctic boundary layer is similar to what has been observed at lower latitudes.

Periods of light winds ($<1\,m\,s^{-1}$ at 11 m) were investigated during the study as well as severe winter storms with wind speeds up to $17\,m\,s^{-1}$. Strong surface thermal inversions as great as $30°\,C \cdot (100\,m)^{-1}$ were measured up to a height of 17 m. Doppler acoustic sounder wind profiles indicate that these inversions ex-

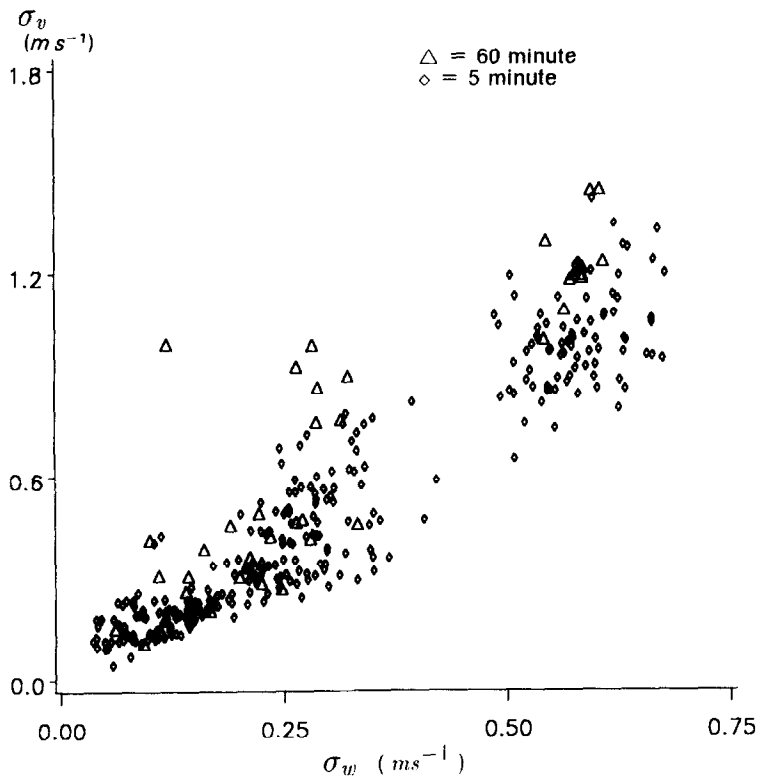

Fig. 16. Standard deviations of horizontal (σ_v) vs vertical (σ_w) wind speed fluctuations at a height of 33 m for 5- and 6-min periods.

tended up to 200 m during light winds. Cooling of the relatively warm marine air at the surface of the snow-covered tundra resulted in the persistence of a weak (1 to 2 °C · (100 m)$^{-1}$) surface inversion in the lowest 10 m even with wind speeds up to 17 m s^{-1}. Profile estimates of surface-layer structure indicate that the Monin–Obukhov length (L) ranges from 4 to 100 m during light wind, very stable conditions and 200 to 1100 m with high wind speeds and $\Delta T/\Delta Z$ between 1 and 2 °C · (100 m)$^{-1}$ The profile method also provides estimates of turbulence production which suggest that shear production dominates and buoyancy effects are small and negative. The large shear production with high wind speeds results in relatively high diffusion rates indicated by the estimated diffusivities which range from 0.5 to 2.9 m^2 · s^{-1}. Spectral analyses of wind direction components also indicate that turbulence production is dominated by shear forces during high winds while buoyancy dissipation appears to be significant with the light wind, strong inversion cases. Estimates of the ratio of friction velocity, u_*, to mean wind speed were similar to values observed at other flat terrain sites, and turbulence intensity scaled with u_* in a manner similar to that observed in other studies. Hourly σ_θ

ranged from 3.2 to 14.8°, with most of the variability due to differences in the amount of low frequency changes in wind direction. Non-Gaussian wind direction distributions and concentration profiles were observed in one third of the hourly averaged data while short-term (5-min) wind direction distributions were always Gaussian. Wind profile power law exponents ranged from 0.06 to 0.14 during high winds and from 0.2 to 0.35 during wind, stable conditions, as expected for a very small surface roughness.

The results of our analyses of arctic open-terrain observations have implications for pollutant dispersion modeling in polar regions. Most of our recommendations based on these data collected in the arctic can be extrapolated to similar sites in the lower latitudes. One exception is that the time of day provides no indication of stability in polar regions during winter. Use of the Pasquill–Gifford curves will always introduce uncertainty by providing discrete rather than continuous estimates of diffusion coefficients. The use of a diffusion estimate with a 10-min averaging time, such as the Pasquill–Gifford estimate, to predict hourly σ_y can underestimate hourly-averaged horizontal diffusion by as much as a factor of 5 by neglecting the effects of low frequency plume meandering. The variance of wind velocity or direction fluctuations provides a more direct measure of turbulence and has a good fit to a Gaussian distribution for time periods up to 5 min. Because wind direction fluctuations frequently did not fit a Gaussian distribution for longer (1–hr) time periods, the non-Gaussian hourly plume profiles should be modeled by calculating sequential short-term (5-min) concentrations and constructing hourly distributions by averaging the short-term results. The somewhat weak correlation between vertical and horizontal turbulence observed during this study, even for 5-min periods, leads us to conclude that the σ_z used in these sequential short-term calculations should be based on a direct measure of vertical turbulence, if σ_w or σ_ϕ is available, or by using a stability classification system which includes both thermal and wind shear effects (L or Ri).

Acknowledgements

This work was funded by the U.S. Environmental Protection Agency (US EPA) (CR 812775-01) through the EPA Cold Climate Research Program. The contents of this paper do not necessarily reflect the views and policies of the US EPA, nor does mention of trade names or commercial products constitute endorsement or recommendation for use. The authors would like to thank G. Allwine, L. Bamesberger, F. Menzia, H. Howard, H. Peterson, B. Friedman, M. Lucachick, and K. Schilling for enduring the harsh arctic environment while assisting in the collection of these data. We are grateful for the assistance provided by employees of the Standard Alaska Production Company and the cooperation of the Alaska Department of Environmental Conservation. We would also like to thank Dr. Peter Finkelstein, US EPA, for his support and guidance as Project Officer.

References

Berkowicz, R. and Prahm, L.: 1982, 'Evaluation of the Profile Method for Estimation of Surface Fluxes of Momentum and Heat', *Atmos. Environ.* **16**, 2809–2819.

Dalrymple, P., Lettau, H., and Wallaston, S.: 1966, 'South Pole Micrometeorology Program: Data Analysis', in M. Rubin (ed.), *Studies in Antarctic Meteorology*, American Geophysical Union Publication 1482, Washington DC.

Deacon, E.: 1973, 'Geostrophic Drag Coefficients', *Boundary-layer Meteorol.* **5**, 321–340.

Draxler, R. R.: 1976, 'Determination of Atmospheric Diffusion Parameters,' *Atmos. Environ.* **10**, 99–105.

Guenther, A., Allwine, E., Bamesberger, L., Friedman, B., and Lamb, B.: 1988, 'Dispersion Modeling in the Arctic', Quality Assurance Final Report (CR812775) to ASRL-EPA, Research Triangle Park, NC.

Guenther, A., Lamb, B., and Petersen, R.: 1989a, 'Modeling of Plume Downwash and Enhanced Diffusion near Buildings: Comparison to Wind Tunnel Observations for an Arctic Industrial Site', *J. Appl. Meteorol.* **28**, 343–353.

Guenther, A., Lamb, B., and Allwine, E.: 1989b, 'Building Wake Dispersion at an Arctic Industrial Site: Field Tracer Observations and Plume Model Evaluations', (submitted to *Atmos. Environ.*).

Hanna, S.: 1986, 'Lateral Dispersion from Tall Stacks', *J. Clim. Appl. Meteorol.* **25**, 1426–1433.

Hanzlick, D., Schrader, G., and Hachmeister, L.: 1988, 'Ice Breakup/Freezeup', 1987 Endicott Environmental Monitoring Program, Envirosphere Co., Anchorage, AK.

Irwin, J.: 1979, 'A Theoretical Variation of the Wind Profile Power-law Exponent as a Function of Surface Roughness and Stability', *Atmos. Environ.* **13**, 191–194.

Kaimal, J., Wyngaard, J., Izumi, Y., and Coté, O.: 1972, 'Spectral Characteristics of Surface-layer Turbulence', *Quart. J. R. Meteorol. Soc.* **98**, 363–589.

Kaimal, J., Eversole, R., Lenschow, D., Stankov, B., Kahn, P., and Businger, J.: 1982, 'Spectral Characteristics of the Convective Boundary Layer over Uneven Terrain', *J. Atmos. Sci.* **39**, 1098–1114.

Lamb, B. and Allwine, G.: 1986, 'Vertical Meteorological Profiles and Wind Fluctuations in the Arctic Surface Boundary Layer', Paper presented at 67th Annual Meeting of the Pacific Division, AAAS, Vancouver, BC.

Lumley, J. and Panofsky, H.: 1964, *The Structure of Atmospheric Turbulence*, Wiley-Interscience, New York.

Panofsky, H. and Dutton, J.: 1984, *Atmospheric Turbulence*, Wiley-Interscience, New York.

Pasquill, F. and Smith, F.: 1983 *Atmospheric Diffusion*, Ellis Horwood Ltd., West Sussex, England.

Rickel, C., Lamb, B., Guenther, A., and Allwine, E.: 1989, 'An Infrared Method for Plume Rise Visualization and Measurement', (submitted to *Atmos. Environ.*).

Sedefian, L. and Bennett, E.: 1980, 'A Comparison of Turbulence Classification Schemes', *Atmos. Environ.* **14**, 741–750.

Vinnichenko, N., Pinus, N., Shmeter, S., and Shur, G.: 1980, *Turbulence in the Free Atmosphere*, Consultants Bureau, New York.

Walker, D. and Webber, P.: 1979, 'Relationships of Soil Acidity and Air Temperature to the Wind and Vegetation at Prudhoe Bay, Alaska', *Arctic* **32**, 224–236.

Weller, G. and Holmgren, B.: 1974, 'The Microclimates of the Arctic Tundra', *J. Appl. Meteorol.* **13**, 854–862.

Wexler, H.: 1936, 'Cooling in the Lower Atmosphere and the Structure of Polar Continental Air', *Mon. Wea. Rev.* **64**, 122–136.